7 The single-particle shell model and nuclear moments

In the previous chapter it has been seen that despite the strength of the interaction between nucleons, it is possible to envisage independent particle motion within nuclear matter. Obviously, the effect of surrounding nucleons cannot be completely forgotten and a realistic discussion of nuclear properties must certainly take account of the pairing interaction at least. Despite this, a simple nuclear model based on the concept of the motion of non-interacting fermions in a spherically symmetrical potential well with a mean free path greater than the radius of the system, has been extremely useful in coordinating a wide range of nuclear phenomena. The model was developed from earlier proposals by Mayer and by Haxel, Jensen and Suess in 1949; since for a spherical system the basic states have wavefunctions that are eigenfunctions of the angular momentum operator, both orbital and total angular momentum are of crucial significance and lead to the definition of the quasi-atomic shells and subshells from which the model takes its name.

In this chapter the empirical evidence that strongly suggests the relevance of shell structure in nuclei will be reviewed, and the simplest interpretation in terms of a potential model will be presented. Some inadequacies of the single-particle model will be mentioned as an introduction to the extended models discussed in Chapter 8. The importance of the single-particle shell model in defining the nucleon configurations from which realistic wavefunctions of nuclear states are constructed will be indicated.

7.1 Empirical evidence for the regularity of nuclear properties

7.1.1 Nuclear mass and binding energy

Although the total binding energy of nuclei is not greatly affected by the character of the motion of the last few ('valence') nucleons, discontinuities are seen when accurately measured masses are compared with the predictions of a smoothly varying mass formula, e.g. equation (6.10). Figure 7.1 shows a plot of this difference against

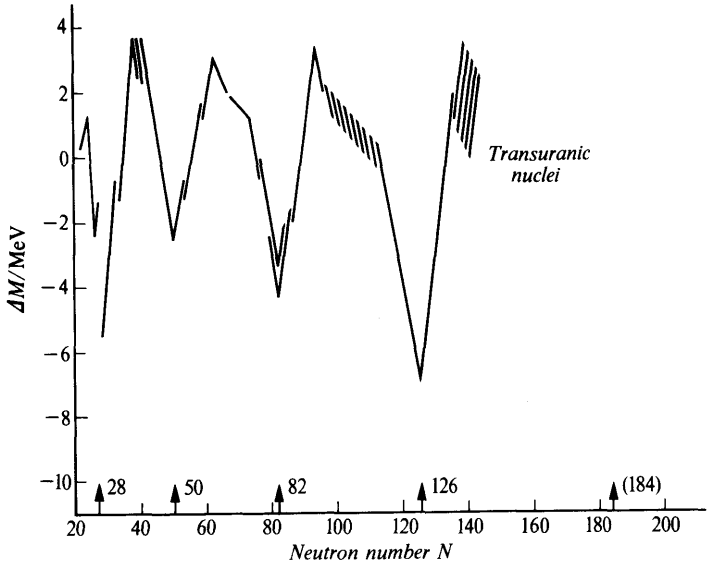

Fig. 7.1 Periodicity of the nuclidic masses. ΔM is the observed mass less that predicted by a smoothly varying formula (adapted from Kümmel, H. *et al.*, *Nuclear Physics*, **81,** 129, 1966).

neutron number and discontinuities are seen at $N = 28$, 50, 82 and 126. This type of effect is reminiscent of the periodicity seen in plots of atomic ionization potentials against atomic number, and like that effect, is interpreted as due to the formation of closed shells of particles. A similar periodicity at the same nucleon numbers up to 82 is seen if nuclidic mass differences are displayed as a function of atomic number Z, so protons and neutrons behave similarly in this respect.

The same discontinuities are seen, without reference to the empirical mass formula, in the nucleon separation energies S_n, S_p. The neutron separation energy S_n near $N = 82$ is shown in Fig. 7.2; for N values just above 82 the separation energies are lower, allowing for pairing effects, than for N just less than 82.

Abundance data, reflecting nuclear stability, have already been mentioned (Sect. 6.6). There is correlation with neutron numbers $N = 50$, 82 and 126 in the sense that nuclides with slightly greater N values are relatively less abundant (Fig. 6.7) and this is again a manifestation of shell closure. The number of isotopes and isotones as a function of Z or N gives similar evidence and additionally indicates that the potential wells are similar for neutrons and protons since the favoured nucleon numbers are the same in each case.

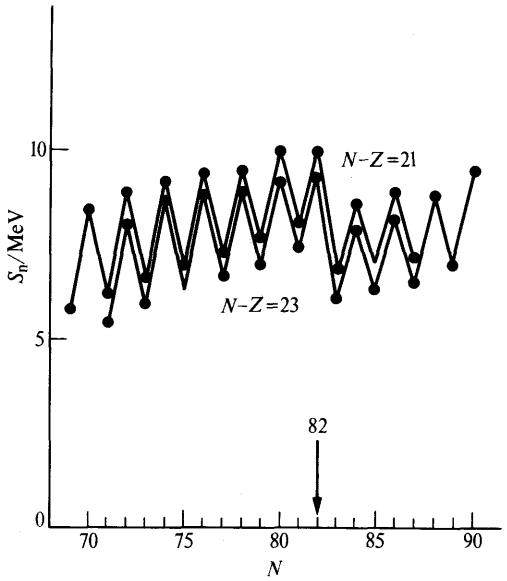

Fig. 7.2 Neutron separation energies near $N=82$. The lines join nuclides of constant neutron excess $N-Z$. The values are calculated from equation (6.4a) and show odd–even staggering. Reproduced from *Nuclear Structure*, Vol. I, 1969, by Aage Bohr and Ben R. Mottleson with permission of the publishers, Addison-Wesley/W. A. Benjamin Inc.

The semi-empirical mass formula predicts the energy release in α- and β-decay to be a smooth function of A. In fact, these energies show non-monotonic variations, although this is essentially the same effect as that shown in Fig. 7.1.

The striking effects of corrections that must be ascribed to shell structure on the barriers impeding the fission of heavy nuclei are recent and strong evidence for the shell model. The double-humped barrier, leading to dynamical effects sometimes known as fission isomerism, will be described later (Sect. 11.7).

7.1.2 Nuclear levels and moments

Even–even nuclei, in which nucleons are paired, are best for displaying systematic effects. Their ground states without exception have spin zero and even parity ($I^\pi = 0^+$) and in most examples the first excited state has $I^\pi = 2^+$. The excitation energy of these 2^+ states gradually decreases with increasing A but also shows maxima at shell closures.

Another special class of nuclear levels showing periodicity is that of the isomeric states (Sect. 9.2.2). These are β- or γ-decaying states for which the radiative transition is of long life because of low

energy or large spin change. The states occur in well-defined groups below the 'magic numbers' (Fig. 9.6).

At higher excitations, the density of nuclear levels also shows shell effects, closed-shell nuclei having a much smaller density because of the extra energy required to change the state of motion of a core nucleon.

The ground state spins and parities of nuclei and their electromagnetic moments show changes that are sometimes abrupt at shell closures. This is a consequence of a basic change of wavefunction.

7.1.3 Conclusion

The evidence presented in preceding sections of the present chapter suggests that nuclei containing 20, 50, 82 or 126 neutrons or protons are particularly stable. Some phenomena also suggest the addition of the number 28. Before considering how the shell model is able to predict these 'magic numbers' we examine some direct evidence for the model that has become available in recent years.

7.1.4 Direct evidence for nuclear shells

The existence of independent particle motion in nuclei has received striking confirmation by the direct observation of proton–hole states through the (p, 2p) reaction. In this process protons of energy 50–400 MeV are used to bombard a nucleus, e.g. ^{12}C, producing a *knock-out* direct reaction

$$^{12}C + p \rightarrow {}^{11}B + 2p \qquad (7.1)$$

The outgoing proton energies are measured in coincidence and geometrical conditions can be imposed which minimize energy loss to the recoil nucleus ^{11}B. The overall loss of energy in the reaction then measures the binding of the knocked-out proton in the ^{12}C nucleus. Figure 7.3 shows some results obtained for this nucleus in the form of a scatter plot relating the energy of one proton to that with which it is associated in the reaction. The distinct band at 45° to the axis indicates that for these events the sum of the proton energies is constant and this means that there is a well-defined binding energy (here ≈ 16 MeV) for the struck proton; for ^{12}C this is interpreted as the energy necessary to form a hole in a p-shell ($l = 1$). The figure also shows a much broader distribution, corresponding with binding energies between 30 and 40 MeV which may be associated with the formation of holes in the s-shell ($l = 0$). The width of the distributions arises because the single-hole states are, in fact, fragmented, in the sense that their strength is spread over a range of states in the nuclear spectrum; the distribution in fact gives the *strength function* (Sect. 11.3) for the hole states.

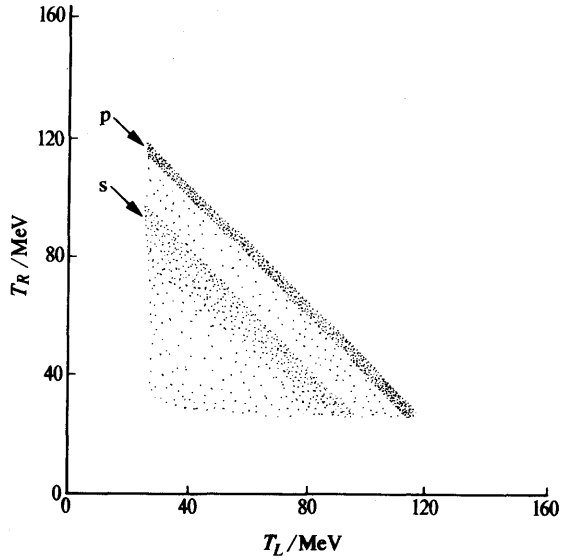

Fig. 7.3 Scatter plot of the energies T_L, T_R of proton pairs from the ^{12}C (p, 2p)^{11}B reaction observed at ±42·5° with a beam of 160-MeV protons (adapted from Gottschalk, B. *et al.*, *Nuclear Physics*, **A90,** 83, 1967).

By altering the angle with respect to the incident beam at which the two protons are observed, the momentum distribution of the struck proton may be explored and the angular momentum of the corresponding bound state may be inferred. The results are consistent with the p and s assignments for ^{12}C. Similar results have been obtained for other and heavier nuclei and with other bombarding particles, including electrons. Evidence for other angular momentum states has been obtained and altogether this type of reaction offers entirely convincing evidence for the existence of independent-particle motion within nuclei.

Single-particle states can also be investigated by the formation of hypernuclei (Sect. 2.4). If a nuclear neutron is changed to a Λ-particle by the reaction $K^-(n, \pi^-)\Lambda^0$ the energy spectrum of the outgoing π^- gives the binding energy of the Λ in the target nucleus. This spectrum has peaks corresponding with the neutron states, at least for light nuclei.

7.2 The single-particle shell model

7.2.1 Objectives

The first objective of the model is clearly to understand how the magic stability numbers of 20, 28, 50, 82 and 126 neutrons or

protons arise. To these numbers it is usual to add 2 (the alpha particle) and 8 (oxygen-16) although these are numbers that arise very naturally among the light nuclides because of the simple nature of $l=0$ and $l=1$ levels, already known in atomic physics. If a satisfactory orbital sequence can be established then the regular filling of orbits in accordance with the Pauli principle will be expected to account for the main features of the properties discussed in Section 7.1.2.

A second objective is to ensure that the potential well adopted to account for the sequence of orbits is consistent with the observed binding energies of the single-particle levels, including virtual levels, and with the general properties of nuclear matter as determined by the internucleon interaction.

Finally, the model must indicate the directions in which it may be improved.

7.2.2 Sequence of orbits

The starting-point of all shell models is the solution of the Schrödinger equation for a particle moving in a spherically symmetrical *central* field of force, i.e. in a field in which the potential energy V of the particle with respect to the centre is a function $V(r)$ of radial distance r only. This problem has been examined generally in Section 1.4, with specific attention to the Coulomb and harmonic oscillator potentials.

Neither of these potentials produces shell closures at the magic numbers, and the same is true of other simple well shapes such as the square well. For the pure harmonic oscillator, for instance, the level order indicated in Section 1.4.2 is

$$(n, l)\text{: 1s; 2p; 2s, 3d; 3p, 4f; . . .}$$

where n is the principal quantum number, or if n is redefined to be the radial quantum number n_r

$$(n, l)\text{: 0s; 0p; 1s, 0d; 1p, 0f; . . .}$$

which gives shell closures at particle numbers

$$2, 8, 20, 40, 70, 112 \tag{7.2}$$

The average spacing of these levels can be obtained by choosing the basic oscillator frequency ω so that the expectation value of r^2 is equal to the mean-square nuclear radius (cf. Ex. 7.7). This gives

$$\hbar\omega \approx 40A^{-1/3}\,\text{MeV} \tag{7.3}$$

and this expression is useful in tracing the systematics of single-particle states.

An essential addition to the shell-model potential, made in 1949 by Mayer and by Haxel, Jensen and Suess was a velocity-dependent term usually known as the *spin-orbit* coupling. Such an effect has already been noted as a necessary component of the two-nucleon interaction (Sect. 5.7). Within the constant-density nuclear volume a force such as this may be expected to average out, but in the nuclear surface there is a density gradient and, therefore, a direction with respect to which the orbital angular momentum $\boldsymbol{r}\times\boldsymbol{p}$ of a single nucleon may be defined. The assumption is that the spin-orbit potential depends on the relative direction of the orbital vector and the intrinsic spin vector so that it may be written

$$V_{ls}(r) = V_{ls}\left(\frac{\hbar}{m_\pi c}\right)^2 \boldsymbol{l}\cdot\boldsymbol{s}\left(\frac{1}{r}\cdot\frac{\mathrm{d}f}{\mathrm{d}r}\right) \tag{7.4}$$

where f gives the profile of the central potential (see eqn (7.12)) and $\boldsymbol{l}$, $\boldsymbol{s}$ are the orbital and spin momenta divided by $\hbar$. The radial factor arises naturally if the nucleon–nucleus spin-orbit potential is derived (Ref. 6.2) from the two-body spin-orbit potential V_{LS} of equation (5.68); the Compton wavelength of the pion is introduced for dimensional reasons.

The spin-orbit doublet levels for a single nucleon have total angular momentum quantum numbers given by

$$j = l \pm \tfrac{1}{2} \tag{7.5}$$

Since the observed spacing between the two components of the doublet is given (Ref. 6.2) by

$$E_{(l+1/2)} - E_{(l-1/2)} = -10(2l+1)A^{-2/3}\,\mathrm{MeV} \tag{7.6}$$

it is necessary that the state with the larger j shall be the more stable. It is also necessary that the splitting shall increase with l (Exs. 7.4 and 7.6). Such a large displacement cannot originate in electromagnetic effects, as it does in atomic spectra.

With these specific assumptions about the spin-orbit coupling the states of the oscillator potential are enumerated as follows:

$$(nl_j)\colon\ 0s_{1/2};\ 0p_{3/2}0p_{1/2};\ 0d_{5/2}1s_{1/2}0d_{3/2};\ 0f_{7/2};\ 1p_{3/2}0f_{5/2}1p_{1/2}0g_{9/2};\ \ldots$$

where n is the radial quantum number n_r, or using the serial number (n_r+1) which indexes the order of appearance of a particular l-value in the level sequence:

$$(nl_j)\colon\ 1s_{1/2};\ 1p_{3/2}1p_{1/2};\ 1d_{5/2}2s_{1/2}1d_{3/2};\ 1f_{7/2};\ 2p_{3/2}1f_{5/2}2p_{1/2}1g_{9/2};\ \ldots \tag{7.7}$$

This order assumes that some anharmonicity or deviation from the pure oscillator-well shape already lowers the states of high angular momentum for a given oscillator number. Each state of given j may

accommodate $(2j+1)$ neutrons and $(2j+1)$ protons, although the well parameters will differ for these two particles.

The scheme (7.7), which will be used in the book, shows that the $1g_{9/2}$ level ($N=4$) is lowered so much by the spin-orbit attractive force that it merges with the levels of oscillator number $N=3$, of opposite parity and similarly for higher N-values. Major shell closures, giving a substantial energy separation, then occur at neutron or proton numbers

$$2, 8, 20, 28, 50, 82, 126 \qquad (7.8)$$

as required by experiment. Between these magic numbers, other shells (subshells) will be completed, with smaller energy differences. The sequence of levels is shown for neutrons or protons in Fig. 7.4 for a well intermediate in shape between a harmonic oscillator and a square well. When both neutrons and protons complete a major shell we speak of a *double-closed-shell* nucleus, e.g. $^{40}_{20}$Ca, $^{208}_{82}$Pb.

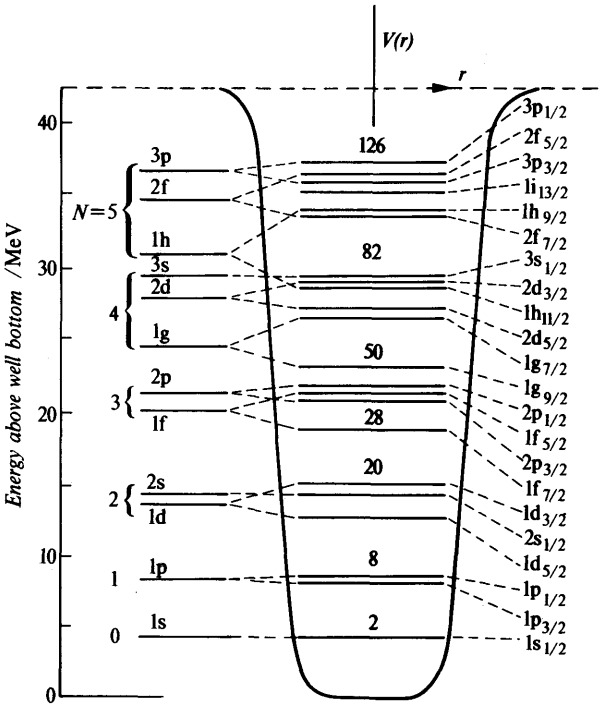

Fig. 7.4 Single-particle levels in a potential well, allowing for spin–orbit coupling. If this effect is sufficient to overcome the oscillator spacing, the magic numbers result.

Continuation of the shell structure shown in Fig. 7.4 to higher nucleon numbers suggests a double-closed shell at $Z = 126$, $N = 184$. However, more detailed considerations (Sect. 11.7.2) indicate that *superheavy elements* of long life against all forms of decay may be found in an 'island of stability' near $Z = 114$, $N = 184$. The nucleus of maximum stability ($^{294}_{110}$X) might have a lifetime comparable with the age of the Earth, and its presence in existing minerals is, therefore, not excluded.

The importance of the simple shell model, apart from giving a general description of nuclear properties in broad outline at least, is that it provides a sequence of single-particle states classified according to n (or n_r), l and j. In atomic spectroscopy, a group of x electrons with the same n- (in this case the principal quantum number) and l-values form a pure *configuration* $(nl)^x$ and the coupling together of their spins and orbital momenta in the Russell–Saunders scheme leads to a number of *terms* denoted by symbols ^{2S+1}L where S is the resultant spin and L is the resultant orbital momentum. The further coupling of spin and orbital vectors to give a resultant J leads to the possible *levels* $^{2S+1}L_J$ and if the magnetic quantum number is specified a level resolves into $2J+1$ *states* $^{2S+1}L_{J,m_J}$. The same definitions can be applied to identical nucleons, but because of the importance of spin-orbit coupling in the shell model a pure configuration specifies the j-value in the form $(nl_j)^x$ e.g. $(2d_{5/2})^3$ and there is no distinction between terms and levels, e.g. $(2d_{5/2})^3_{5/2}$ or $(2d^3_{5/2}; I = \frac{5}{2})$. A state may be written $(2d^3_{5/2}; I = \frac{5}{2}, m_I = \frac{3}{2})$. Unfortunately, it is difficult to confine the usage of the word 'state' to this precise definition; it will often imply a linear combination of terms.

The single-particle shell model asserts that when x is even, the resultant total angular momentum of the lowest term of a pure configuration is zero, because of pairing, and that when x is odd the resultant is equal to the j-value of the configuration.

The succession of nuclei in the N–Z chart may be envisaged in terms of the configurations based on a single-particle potential of slowly varying depth (Sect. 7.2.4) and of a radius increasing with mass number. Neutrons and protons are added in accordance with the Pauli principle to complete the configurations and as the radius increases so it becomes possible for single-particle states of higher n and l to be bound within the potential well. The binding of a new level may produce a change in some property controlled by the single-particle motion, e.g. the ground state spin, and this accounts for the observed periodicities. Changes in scattering or reaction cross-section may also be observed for the same reason.

In an odd-A nucleus the simplest excitations (intrinsic states) are those in which the odd nucleon enters one of the series of single-particle orbits. Such states may be studied by transfer reactions

(Sect. 11.5 and Ref. 7.1) and are seen particularly clearly in nuclei such as $^{209}_{83}$Bi with one proton outside a closed shell ($Z = 82$). If also the excited states of $^{207}_{81}$Tl, with one proton hole, are measured, the whole range of proton states above and within the closed shell may be identified. They are found to follow the order shown in Fig. 7.4, with the exception of an inversion of the $f_{7/2}$ and $h_{9/2}$ states, and clearly show a major shell gap of about 4·5 MeV between the $h_{9/2}$ and $s_{1/2}$ states. The results of a similar study of the neutron states in the nucleus $^{209}_{82}$Pb ($N = 127$) are shown in Fig. 11.11.

In some odd-mass nuclei the sequence of single-particle levels is not followed faithfully because the required excitation involves passage of a particle to another major shell, e.g. $d_{3/2} \rightarrow f_{7/2}$. A more favourable arrangement may be for a pair in a lower subshell (e.g. $s_{1/2}$) to break, and a pair in an upper subshell (e.g. $d_{3/2}$) to form, leaving the configuration $s_{1/2}^{-1}$. The gain of energy from such rearrangements may sometimes be sufficient to allow passage across a shell gap (see Ex. 7.3).

7.2.3 Parity, spin and moments of nuclear ground states

The usefulness of a parity quantum number ($\pm$, or even/odd) is well established in atomic physics and indicates that the electromagnetic interaction is invariant under the space-inversion transformation (Sect. 1.3). In a nucleus, the strong interaction determines the energy levels and again parity is expected to be conserved. Each of these statements must be modified slightly because of a small intrusion of the parity-violating property of the weak interaction (Ch. 10). For nuclear states however, the amplitude of the impurity expected for this reason is only 10^{-6} to 10^{-7} of the regular amplitude of the wavefunction and can usually be disregarded.

The parity of a nuclear state can be measured, relatively at least, by studying reactions such as the neutron transfer collision (deuteron stripping)

$$^{16}\mathrm{O} + \mathrm{d} \rightarrow {}^{17}\mathrm{O} + \mathrm{p} \tag{7.9}$$

The theory of this process (Sect. 11.5) shows how the orbital angular momentum of the transferred neutron can be deduced from the angular distribution of the stripped protons. If this angular momentum is $l\hbar$ then the relative parity of ^{17}O and ^{16}O is $(-1)^l$ since the neutron space wavefunction has an angular dependence $P_l(\cos\theta)$, which changes sign or not under space-inversion according to the l-value. The intrinsic parity of the nucleons is even by convention. Other methods of parity determination are based on the selection rules for radiative transitions (Ch. 9).

The parity of a nucleus as a whole is the product of the parities of the neutrons and protons and is, therefore, determined by the

occupation of the single-particle states predicted by the shell model. There is excellent agreement with the model, e.g.

for $A = 6$, $1s^4 1p^2$, parity even (+)
for $A = 7$, $1s^4 1p^3$, parity odd (−)
for $A = 19$, closed shell +(2s or 1d)^3, parity even (+)

Nuclear spins are small integral multiples of the fundamental spin $\frac{1}{2}\hbar$, which is known experimentally to be the spin of both proton and neutron. Spins are determined, often together with magnetic dipole and electric quadrupole moments, by optical hyperfine spectroscopy and by magnetic resonance experiments using both liquids and solids and also collision-free beams of atoms and molecules. The strong tendency of protons and neutrons to pair off suggests, quite independently of specific models, that *even-N–even-Z nuclei have zero ground-state spin.* Additionally, it also follows in a model-independent way, that the spin of an odd-A nucleus is equal to the total resultant angular momentum $\boldsymbol{j} = \boldsymbol{l} + \boldsymbol{s}$ of the odd nucleon, all other pairs being assumed to couple to zero resultant. The spins of ground states of odd-A nuclei change abruptly at the magic numbers, as illustrated for some odd-proton nuclei in Table 7.1. Moreover, odd-mass nuclei with a nucleon number just below a magic value may have single-particle excited states with a spin value considerably different from that of the ground state, e.g. $I_e = \frac{9}{2}$ compared with $I_g = \frac{1}{2}$. This is the reason for isomerism (Sect. 9.2.2) in such nuclei.

Magnetic dipole moments of odd-mass nuclei which are well described by a single-particle model can be predicted by a simple calculation following the derivation of the Landé g-factor in atomic physics. The moment μ_I is given by the equation

$$\mu_I = g_I \mu_N I \tag{7.10}$$

where I is the nuclear spin quantum number, μ_N is the nuclear magneton and g_I is the resultant gyromagnetic ratio given by

$$g_I = \tfrac{1}{2}\left[(g_l + g_s) + (g_l - g_s)\frac{l(l+1) - \frac{3}{4}}{j(j+1)}\right] \tag{7.11}$$

In this expression g_l and g_s are the orbital and intrinsic spin gyromagnetic ratios for the odd nucleon concerned (see Appendix 6) and l and j are the orbital and total angular momentum quantum numbers, the latter being equal to the nuclear spin quantum number I for an odd-mass nucleus.

From observed values of μ_I, with knowledge of I, the l-value and hence the parity of the ground state can be predicted. In general, magnetic moments, although not quantized, change when spin values change and therefore indicate the same periodicity, illustrated in

TABLE 7.1 Properties of selected odd-proton nuclei

l_j is the state of motion of the odd proton. For the deformed nuclei l is not a good quantum number. The symbol I^π gives ground-state spin and parity.

Z	A	*Atom*	l_j	I^π	μ_I/μ_N	Q_I/b	*Predicted configuration of protons* (Fig. 7.4)				
							$1s_{1/2}$	$1p_{3/2}$	$1p_{1/2}$		
1	1	H	$s_{1/2}$	$\frac{1}{2}^+$	2·793	—	1				
3	7	Li	$p_{3/2}$	$\frac{3}{2}^-$	3·256	−0·04	2	1			
7	15	N	$p_{1/2}$	$\frac{1}{2}^-$	−0·283	—	2	4	1		
8											
							$1d_{5/2}$	$2s_{1/2}$	$1d_{3/2}$		
9	19	F	$s_{1/2}$	$\frac{1}{2}^+$	2·629	—	1				
11	23	Na	$(d_{5/2})^3$	$\frac{3}{2}^+$	2·218	0·14	3				
19	39	K	$d_{3/2}$	$\frac{3}{2}^+$	0·391	0·055	6	2	3		
20											
							$1f_{7/2}$				
21	45	Sc	$f_{7/2}$	$\frac{7}{2}^-$	4·756	−0·22	1				
25	55	Mn	$(f_{7/2})^3$	$\frac{5}{2}^-$	3·444	0·4	5				
27	59	Co	$f_{7/2}$	$\frac{7}{2}^-$	4·62	0·4	7				
28											
							$2p_{3/2}$	$1f_{5/2}$	$2p_{1/2}$	$1g_{9/2}$	
29	63	Cu	$p_{3/2}$	$\frac{3}{2}^-$	2·223	−0·18	1				
31	69	Ga	$p_{3/2}$	$\frac{3}{2}^-$	2·016	0·19	3				
35	79	Br	$p_{3/2}$	$\frac{3}{2}^-$	2·106	0·31	4	3			
47	107	Ag	$p_{1/2}$	$\frac{1}{2}^-$	−0·114	—	4	6	1		
49	113	In	$g_{9/2}$	$\frac{9}{2}^+$	5·523	0·82	4	6	2	9	
50											
							$1g_{7/2}$	$2d_{5/2}$	$1h_{11/2}$	$2d_{3/2}$	$3s_{1/2}$
51	121	Sb	$d_{5/2}$	$\frac{5}{2}^+$	3·359	−0·29	1				
51	123	Sb	$g_{7/2}$	$\frac{7}{2}^+$	2·547	−0·37	1				
63	151	Eu	$d_{5/2}$	$\frac{5}{2}^+$	3·464	1·1	8	5			
67	165	Ho	—	$\frac{7}{2}^-$	4·12	3·0					
71	175	Lu	—	$\frac{7}{2}^+$	2·23	5·6	Deformed nuclei				
73	181	Ta	—	$\frac{7}{2}^+$	2·36	4·2					
75	185	Re	$d_{5/2}$	$\frac{5}{2}^+$	3·172	2·7	8	6	11		
79	197	Au	$d_{3/2}$	$\frac{3}{2}^+$	0·145	0·58	8	6	12	3	
81	203	Tl	$s_{1/2}$	$\frac{1}{2}^+$	1·612	—	8	6	12	4	1
82											
							$2f_{7/2}$	$1h_{9/2}$	$3p_{3/2}$	$2f_{5/2}$	
83	209	Bi	$h_{9/2}$	$\frac{9}{2}^-$	4·080	−0·35	1				

Notes: [1] For ^{19}F, ^{79}Br, ^{121}Sb, ^{185}Re and ^{209}Bi deviations from the level order of Fig. 7.4 are seen.
[2] For ^{23}Na and ^{55}Mn the observed spin must be explained by coupling of equivalent nucleons or by deformation (Ch. 8).

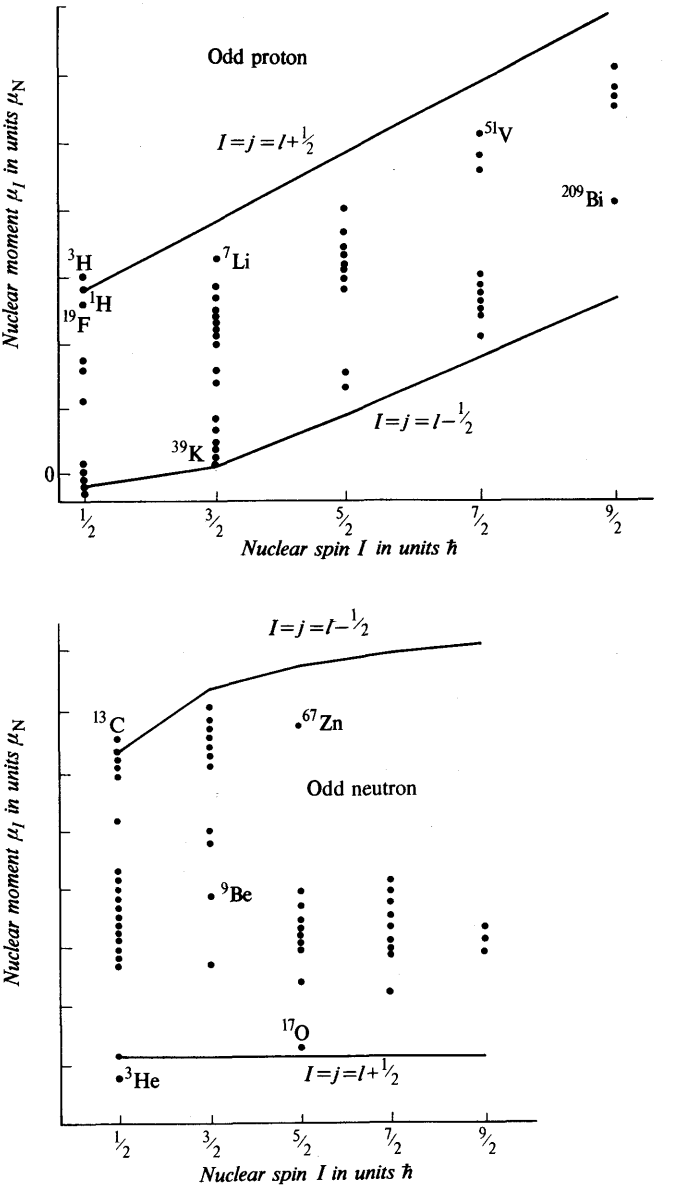

Fig. 7.5 Schmidt diagrams showing magnetic moment of odd-mass nuclei as a function of nuclear spin. The lines show the magnetic moments expected for a single nucleon at the spin values $j = l \pm \frac{1}{2}$. (Blin-Stoyle, R. J., *Theories of Nuclear Moments*, OUP, 1957).

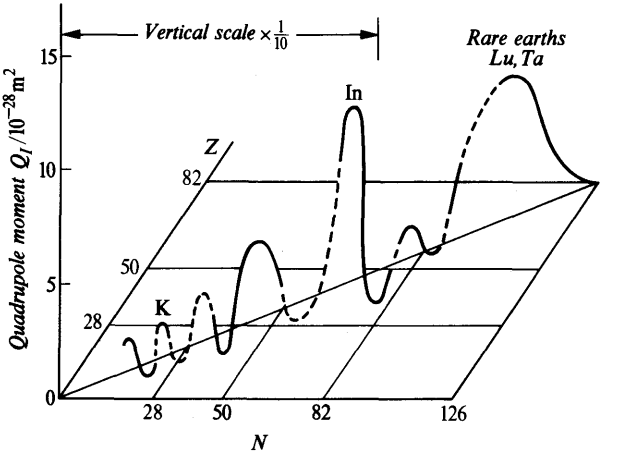

Fig. 7.6 Values of nuclear electric quadrupole moment Q_I as a function of N and Z. (Kopferman, H., *Nuclear Moments*, Academic Press, 1958).

Table 7.1. In detail, however, nuclear moments do *not* agree with simple predictions of equations (7.10) and (7.11) for odd-mass nuclei; the experimental results are given in Fig. 7.5. This displays the so-called Schmidt lines which result from the extreme single-particle prediction. Evidently, real nuclei are such that pure single-particle motion is in many cases diluted.

Electric quadrupole moments Q_I also show a periodicity, e.g. a change of sign at shell closures, as illustrated in Table 7.1 and Fig. 7.6. The outstanding features of this property, however, are:

(*a*) its existence at all for nuclei of the type of ^{17}O, which might be supposed to be a neutron attached to a spherical symmetrical ^{16}O core; and

(*b*) the very large values, in comparison with single-particle expectations, found for the group of rare earth nuclei.

These observations indicate an enhancement of single-particle motion, namely a collective effect (Ch. 8).

7.2.4 *The average shell-model potential*

Because of the short range of internucleon forces the radial shape of the shell-model potential may be expected to resemble the charge density distribution given by equation (6.8a). The main central nuclear potential may then be written

$$\begin{aligned} V(r) &= -V_0[1+\exp{(r-R_V)/a}]^{-1} \\ &= -V_0 f(r, R_V, a) \end{aligned} \tag{7.12}$$

where $f(r, R_V, a)$ is known as the Saxon–Woods *form factor*. The parameters R_V and a are not necessarily the same as those for the charge distribution because for the potential energy the range of nucleon–nucleon forces must be included (Sect. 6.2). The radial shape differs from the harmonic oscillator shape in such a way that the remaining l-degeneracy (Sect. 1.4.2) is removed and the levels of higher l for a given N are lowered in energy.

The potential well of the single-particle model may be expected to reflect some of the features apparent in the semi-empirical mass formula, to which it must contribute. The main correction to a constant well depth is an asymmetry potential proportional to $\pm T_z/A$ to represent the fact that neutrons and protons feel different forces on the average; the presence of an asymmetry term proportional to T_z^2/A in the mass formula will be recalled. There is also a Coulomb term $V_C(r)$ with the radial dependence of a point-charge field outside the nucleus, which lifts the proton well with respect to that for neutrons. Finally, a spin-orbit term $V_{ls}(r)$ as given in (7.4) must be added; it may also contain an asymmetry term.

The potential may in principle be determined by calculating the binding of the single-particle states and comparing them with experiment. Because of residual interactions so far neglected, no very precise results can be expected from this approach. This is already evident from the spread of binding energies seen in the (p, 2p) experiments. A more powerful approach is to probe the potential well through scattering experiments

The first approach of this sort was an examination of slow-neutron scattering lengths a as a function of A. If the neutron–nucleus interaction were adequately represented by a hard sphere of radius $R = r_0 A^{1/3}$ a smooth variation of a with A would be expected as shown in Fig. 7.7; in fact, discontinuities appear due to the binding of new s-orbits within a potential well at particular values of the parameter KR, where K is the internal wavenumber. It has already been noted that a bound state at zero energy implies an infinite scattering length (Sect. 5.2.2), in accordance with the trend of the results sketched in Fig. 7.7. The scattering anomalies in slow-neutron cross-sections are also in conflict with the assumption that a nucleus acts as a black, or strongly absorbing sphere. All available evidence, however, is consistent with the existence of a well of depth ≈ 50 MeV with the property of both absorbing and scattering an incident particle.

For scattering problems, involving unbound states, the shell-model potential with its absorptive and refractive properties is known as the *optical* potential. It has been extensively studied, especially in the elastic scattering of protons of energy above the Coulomb barrier by a range of nuclei. Figure 7.8 shows some of the differential cross-sections obtained, expressed as a ratio to the

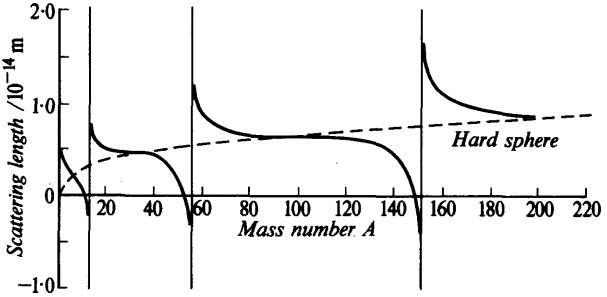

Fig. 7.7 Slow-neutron scattering length as a function of mass number, showing the expectation for hard-sphere scattering (dotted curve) and for scattering by a square-well potential (solid curves). Experimental points follow the latter.

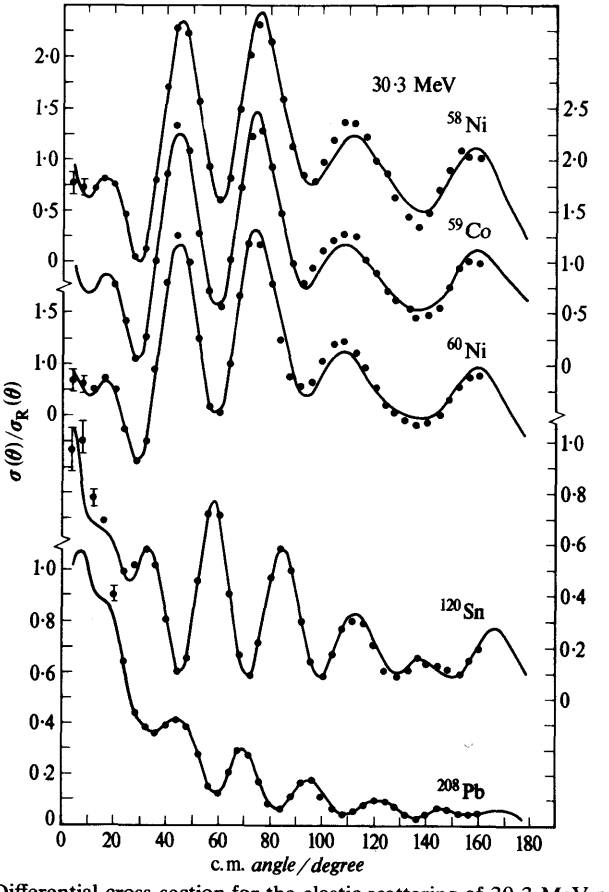

Fig. 7.8 Differential cross-section for the elastic scattering of 30·3-MeV protons by nuclei. The points are experimental and the curves are theoretical fits (Greenlees, G. W. *et al.*, *Phys. Rev.*, **171,** 1115, 1968).

Rutherford scattering from a point charge. The optical potential may be written in just the form of the shell-model potential, but with extra parameters to allow for the different geometrical behaviour (i.e. different form factors) of the various main terms. A frequently used form is:

$$V(r) = V_C(r) - V_0 f_1(r, R_V, a_V) - iW_0 f_2(r, R_W, a_W) + V_{ls}(\hbar/m_\pi c)^2 \boldsymbol{l} \cdot \boldsymbol{s} \left(\frac{1}{r} \cdot \frac{d}{dr}\right) f_3(r, R_{ls}, a_{ls}) \quad (7.13)$$

in which the main terms of the shell-model potential for bound states will be recognized, together with an imaginary term $\approx W_0$ to represent the absorptive effect of the well on the incident particles. The form factors f_1, f_2, f_3 generally have the Saxon–Woods form of equation (7.12).

The computer analysis of results such as those shown in Fig. 7.8 brings many partial waves into the scattering amplitude and yields parameters of the sort shown in Table 7.2. Usually, the radii R are taken to vary as $A^{1/3}$ and the parameter a which measures the surface thickness, is kept independent of A. The spin-orbit potential V_{ls} is found from measurements of polarization effects in the scattering.

The shell-model potential is the extrapolation of the optical potential back to an energy corresponding to a bound particle. The variation with energy of the terms V_0 and W_0 is shown (for neutrons) in Fig. 7.9. Comparison of the real central potential for neutron scattering with that for proton scattering reveals the presence of an isospin-dependent term not shown in (7.13) but already mentioned in connection with the shell-model potential.

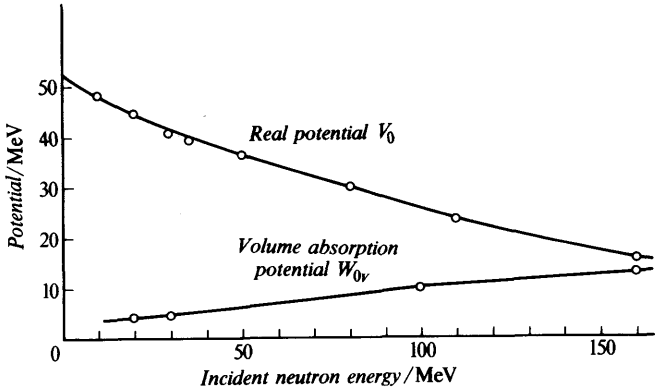

Fig. 7.9 Variation of real and imaginary parts of the optical potential with incident neutron energy.

TABLE 7.2 Optical model analysis of 30·3-MeV proton scattering for a range of nuclei; potentials are given in MeV.

	^{40}Ca	^{58}Ni	^{120}Sn	^{208}Pb
V_0	46·1	47·0	51·1	53·4
W_{0v}	0·4	3·4	1·2	4·0
W_{0s}	5·96	4·4	8·7	7·6
V_{ls}	12·0	8·8	12·0	10·2

The geometrical parameters differ for the different potentials but are approximately

$$R = r_0 A^{1/3},\ r_0 = 1{\cdot}25 \text{ fm}$$

$$a = 0{\cdot}65 \text{ fm}$$

In this particular analysis, taken from the work of Greenlees and Pyle (*Phys. Rev.*, **149**, 836, 1966), the imaginary potential is split into a part W_{0v} representing absorption over the whole nuclear volume and a surface-peaked part W_{0s}. The value of the spin-orbit potential V_{ls} has been adjusted to take account of the use of the actual spin **s** in equation (7.13).

7.2.5 *Bound states*

The spherical potential defined by the scattering experiments should lead to the single-particle levels of the shell model as eigenstates. A detailed calculation (Ref. 6.2) for a potential with just central and spin-orbit terms gives results of the form shown in Fig. 7.10 for the energies of neutron states.

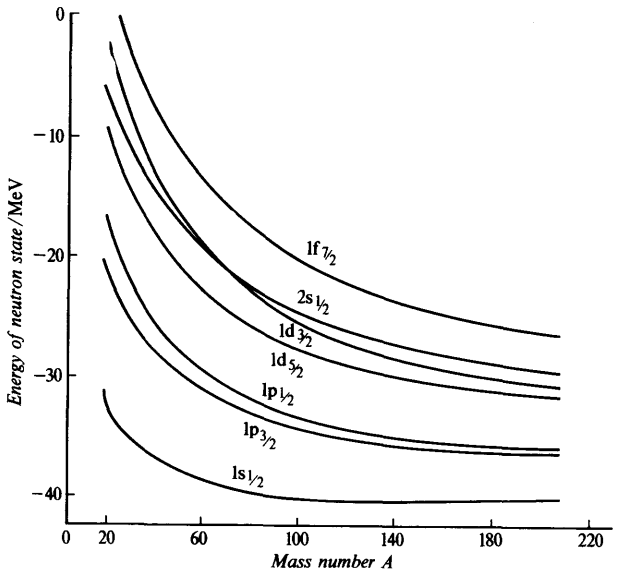

(Figs 7.9 and 7.10 reproduced from *Nuclear Structure*, Vol. I, 1969, by Aage Bohr and Ben R. Mottelson with permission of the publishers, Addison-Wesley/W. A. Benjamin Inc.

The energies calculated in this way are consistent with the general trend of observed level sequences, and with the results of (p, 2p) experiments, but are only a first approach because of the neglect of residual interactions. The eigenfunctions are also consistent with the size parameters found by electron scattering. The calculations show that a state of given (n, l) becomes more tightly bound as A increases, in conformity with the somewhat cruder prediction of single-particle level spacing (7.3).

7.3 Summary

The single-particle shell model, based upon a near-harmonic oscillator potential, gives an excellent account of many nuclear properties, and especially of the periodicity indicated by the 'magic' numbers. The success of the model results from the fact that it takes over from the theory of nuclear matter the concept of single-particle motion within a degenerate Fermi gas, with an effective interaction between nucleons that includes a two-body spin-orbit potential. In finite nuclei the residual interaction contains a significant pairing effect that exposes the last nucleon in odd-A nuclei. Its shortcomings in prediction of electric and magnetic moments arise from a neglect of the correlation between nucleons, apart from pairing.

The shell-model potential is best examined through the elastic scattering of protons and neutrons. The potential and its radial form factors can be made consistent with nucleon separation energies and with the charge distributions sensed by electron scattering experiments. It has been possible through the development of the so-called *folding models* to relate the terms of the optical potential to matter densities with an assumed nucleon–nucleon interaction (Sect. 11.4).

Examples 7

7.1 Using the relativistic relation between momentum and energy find the minimum kinetic energy of (*a*) an electron, (*b*) a proton, confined within a dimension of 7×10^{-15} m. (Assume $\Delta p\times\Delta r=\hbar$). [28, 0·42 MeV]

7.2 Write down the expected odd-particle configuration of the following nuclei:

$$^{27}_{13}\mathrm{Al};\ ^{29}_{14}\mathrm{Si};\ ^{40}_{19}\mathrm{K};\ ^{93}_{41}\mathrm{Nb};\ ^{157}_{64}\mathrm{Gd}.\ [\mathrm{d}_{5/2};\ \mathrm{s}_{1/2};\ \mathrm{d}_{3/2}+\mathrm{f}_{7/2};\ \mathrm{g}_{9/2};\ \mathrm{h}_{9/2}]$$

7.3 Predict the spin-parity of the first excited state of the nuclei $^{31}_{14}\mathrm{Si}$, $^{41}_{19}\mathrm{K}$, $^{49}_{21}\mathrm{S}$. $[\frac{7}{2}^-, \frac{7}{2}^-, \frac{3}{2}^-]$. Comment on the fact that the observed values are $\frac{1}{2}^+$, $\frac{1}{2}^+$, $\frac{3}{2}^+$.

7.4* From the equation $\boldsymbol{j}=\boldsymbol{l}+\boldsymbol{s}$ for a single particle in an eigenstate of the operators $\boldsymbol{j}$, $\boldsymbol{l}$, $\boldsymbol{s}$ obtain the value of the quantity $(\boldsymbol{l}.\boldsymbol{s})$ and show that the energy separation of a nucleon spin-orbit doublet is proportional to $(2l+1)$ (if the radial dependence of V_{ls} is smooth). For the case $l=1$, $j=\frac{3}{2}$, what is the angle between $\boldsymbol{l}$ and $\boldsymbol{j}$? [24°]

7.5 From equation (7.4), using the Saxon–Woods form-factor f given by (7.12), determine and sketch the radial variation of the spin-orbit potential $V_{ls}(r)$.

7.6* Obtain an order-of-magnitude estimate of the spin-orbit energy that would arise due to electromagnetic effects from the motion of a proton in a p-state in a nucleus of $Z = 10$, assuming a central point charge as in the simple theory of the electronic fine structure. Compare your result with the observed spacing given by equation (7.6) for $A = 20$.

7.7* Assuming that the expectation value of the potential energy of a harmonic oscillator state is half the total energy $(N+\frac{3}{2})\hbar\omega$, find the expectation value of the mean-square radius for a nucleon in such a state.

For the case of N large find the value of N for a nucleus containing A nucleons, assuming equal numbers of neutrons and protons.

By equating the summed $\langle r^2 \rangle$ for all the nucleons to $\frac{3}{5}AR^2$ deduce the form of equation (7.3).

7.8* Following the method of Example 7.7, show that the spacing of hypernuclear energy levels is $\hbar\omega \approx 60A^{-2/3}$ MeV.

7.9 The low-lying levels of $^{39}_{20}$Ca have spin-parity values, starting from the ground state, of $\frac{3}{2}^+$, $\frac{1}{2}^+$, $\frac{7}{2}^-$ and $\frac{3}{2}^-$. Interpret these values on the basis of the single-particle shell model.

7.10 The single-particle potential is sometimes written with a term $(\boldsymbol{t}.\boldsymbol{T})/A$ where $\boldsymbol{t}$ is the isospin of a nucleon and $\boldsymbol{T}$ that of the target. Evaluate this term for a nucleus (A, N, Z) in the cases $T_> = T+\frac{1}{2}$, $T_< = T-\frac{1}{2}$.

7.11* Calculate the ground-state magnetic moments of ^{7}Li, ^{23}Na, ^{39}K, ^{45}Sc and compare with the values shown in Table 7.1, which gives the spins of these nuclides.